



Heterogeneous Catalysis Hot Paper

How to cite: *Angew. Chem. Int. Ed.* **2021**, *60*, 5800–5805

International Edition: doi.org/10.1002/anie.202013610

German Edition: doi.org/10.1002/ange.202013610

# Tunable $e_g$ Orbital Occupancy in Heusler Compounds for Oxygen Evolution Reaction\*\*

Mingquan Yu<sup>+</sup>, Guowei Li<sup>+</sup>, Chenguang Fu<sup>+</sup>, Enke Liu, Kaustuv Manna, Eko Budiyo, Qun Yang, Claudia Felser,\* and Harun Tüysüz\*

**Abstract:** Heusler compounds have potential in electrocatalysis because of their mechanical robustness, metallic conductivity, and wide tunability in the electronic structure and element compositions. This study reports the first application of  $Co_2YZ$ -type Heusler compounds as electrocatalysts for the oxygen evolution reaction (OER). A range of  $Co_2YZ$  crystals was synthesized through the arc-melting method and the  $e_g$  orbital filling of Co was precisely regulated by varying Y and Z sites of the compound. A correlation between the  $e_g$  orbital filling of reactive Co sites and OER activity was found for  $Co_2MnZ$  compounds ( $Z = Ti, Al, V, \text{ and } Ga$ ), whereby higher catalytic current was achieved for  $e_g$  orbital filling approaching unity. A similar trend of  $e_g$  orbital filling on the reactivity of cobalt sites was also observed for other Heusler compounds ( $Co_2VZ$ ,  $Z = Sn \text{ and } Ga$ ). This work demonstrates proof of concept in the application of Heusler compounds as a new class of OER electrocatalysts, and the influence of the manipulation of the spin orbitals on their catalytic performance.

Heusler compounds are a large class of intermetallic compounds with the chemical formula  $X_2YZ$  or  $XYZ$  (also known as “half-Heusler”), where  $X$  and  $Y$  are transition

metals,  $Z$  is usually the main group element or a transition metal.<sup>[1]</sup> Owing to the wide tunability in the electronic structure and constituent elements, Heusler compounds have shown plentiful magnetic and electronic functionalities, such as half-metallicity, thermoelectric, superconducting, magneto-caloric, magneto-optical, spin transfer torque characteristics, as well as, topological insulator, magnetic Weyl fermion and magnetic Skyrmion.<sup>[1]</sup> The band gap of Heusler family compounds can be readily tuned from 0 to 4 eV by carefully selecting the chemical composition.<sup>[1–3]</sup> These result in distinctly different electrical transport behaviors from highly conductive metals to insulators. More interestingly, one can even predict and then design the magnetic states of Heusler compounds as their magnetic ordering is strongly dependent on the arrangement of the atoms.<sup>[4]</sup> Taking half-metallic Heusler alloys as an example, the spin channel filling is related to the number of valence electrons. Thereby, the spin magnetic moment can be obtained according to the Slater-Pauling rule in which the number of valence electrons is solely involved.<sup>[5]</sup>

For heterogeneous catalytic reactions such as electrochemical water splitting, high-efficient and economic catalysts based on non-noble metals are required for the scalable hydrogen production. This is particularly important for the oxygen evolution reaction (OER) at the anode, which is thermodynamically sluggish and limiting the overall efficiency of water electrolysis.<sup>[6]</sup> Design of OER electrocatalysts with low overpotential has been an interesting topic to both fundamental research and industrial applications under the framework of hydrogen economy.<sup>[7]</sup> For OER catalysis, the adsorption of various reaction intermediates on the surface of catalysts is a key step. The adsorption behaviors are governed by the electronic structures of the investigated catalyst.<sup>[8]</sup> The Shao-Horn group reported the correlation between intrinsic activity and  $e_g$  orbital filling of transition metal cations in a series of perovskite catalysts.<sup>[9]</sup> A universal principle was thus put forward using  $e_g$  orbital filling as an activity descriptor, namely the Shao-Horn (SH) principle. It was proposed that  $e_g$  orbital filling influences the binding energy of oxygen intermediates to the catalyst surface, and as a result alters the OER activity. Accordingly, SH principle points out a rational way to optimize OER catalysts, which is based on tuning the  $e_g$  orbital filling of metal sites.<sup>[10]</sup> So far, most reported works adopted a rather similar strategy of introducing vacancies through heteroatom doping.<sup>[8,11]</sup> Although it has been demonstrated to be effective to regulate  $e_g$  electron configuration of various transition metal compounds, a new class of materials, like Heusler compounds, with precisely

[\*] Dr. M. Yu,<sup>[+]</sup> E. Budiyo, Priv.-Doz. Dr. H. Tüysüz  
Max-Planck-Institut für Kohlenforschung  
Kaiser-Wilhelm-Platz 1, 45470 Mülheim an der Ruhr (Germany)  
E-mail: tueysuez@kofo.mpg.de

Dr. G. Li,<sup>[+]</sup> Dr. C. Fu,<sup>[+]</sup> Prof. E. Liu, Dr. K. Manna, Q. Yang,  
Prof. Dr. C. Felser  
Max Planck Institute for Chemical Physics of Solids  
Nöthnitzer Straße 40, 01187 Dresden (Germany)  
E-mail: Claudia.Felser@cpfs.mpg.de

Prof. E. Liu  
Beijing National Laboratory for Condensed Matter Physics, Institute  
of Physics, Chinese Academy of Sciences  
Beijing, 100190 (P. R. China)

Dr. K. Manna  
Department of Physics, Indian Institute of Technology  
Delhi, New Delhi 110016 (India)

[+] These authors contributed equally to this work.

[\*\*] A previous version of this manuscript has been deposited on a preprint server (<https://doi.org/10.26434/chemrxiv.13072910.v1>).

Supporting information and the ORCID identification number(s) for the author(s) of this article can be found under:  
<https://doi.org/10.1002/anie.202013610>.

© 2020 The Authors. Angewandte Chemie International Edition published by Wiley-VCH GmbH. This is an open access article under the terms of the Creative Commons Attribution License, which permits use, distribution and reproduction in any medium, provided the original work is properly cited.

controlled  $e_g$  orbital filling is a stimulating platform for further development of OER catalysts.

Intermetallic compounds with transition metals as the constituents have attracted increasing attention for the discovery of new catalysts and the investigation of catalytic mechanisms. In this regard, Heusler compounds could be a potential new platform which however was rarely noticed in the catalysis community. Until recently, Kojima et al. reported selective hydrogenation of alkyne over  $\text{Co}_2\text{MnGe}$  and  $\text{Co}_2\text{FeGe}$ , demonstrating the potential of Heusler compounds as new catalysts.<sup>[12]</sup> Interestingly, the metallic conductivity and multi-metal constituent of Heusler compounds resemble high entropy alloys that were discovered as promising OER catalysts several years ago.<sup>[13,14]</sup> Therefore, Heusler compounds with designed tunability of  $e_g$  electron configuration, metallic conductivity, and multi-metal constituent, show great potential as a new class of catalyst for OER.

In this work, to the best of our knowledge, we report the first study of Heusler compounds as novel electrocatalysts towards the OER. Heusler compounds ( $\text{Co}_2\text{MnZ}$ ) with high crystallinity and homogeneous element distribution were prepared by the arc-melting method. The  $e_g$  electron configuration of reactive Co sites was precisely regulated by varying unreactive metal sites ( $Z = \text{Ti, Al, Ga, V}$ ). A solid correlation between the  $e_g$  orbital filling of reactive sites and OER activity was found on  $\text{Co}_2\text{MnZ}$  compounds whereby higher catalytic current was achieved on the catalyst when  $e_g$  orbital filling approaches to unity. Furthermore, another set of Heusler compounds ( $\text{Co}_2\text{VZ}$ ) were prepared and their OER activity demonstrates the volcano-shaped dependence on  $e_g$  orbital filling of reactive Co sites.

$\text{Co}_2\text{YZ}$  Heusler compounds are crystallized in the cubic structure  $Fm\bar{3}m$  (space group no. 225) with  $\text{Cu}_2\text{MnAl}$  ( $L2_1$ ) as a prototype. As exhibited in Figure 1 a, Co, Y, and Z atoms occupy the Wyckoff position  $8c$  ( $1/4, 1/4, 1/4$ ),  $4b$  ( $1/2, 1/2, 1/2$ ), and  $4a$  (0, 0, 0), respectively. The electrical and magnetic properties of Heusler compounds can be simply connected to their valence electron number  $N_v$ . Generally, Heusler compounds with  $N_v$  of 24 show a semiconducting behavior, where compounds with a larger or smaller  $N_v$  exhibit metallic behavior and magnetism. The magnetic moment  $M$  of  $\text{Co}_2\text{YZ}$  Heusler compounds with four atoms per unit cell follows the Slater-Pauling rule, i.e.,  $M = (N_v - 24) \mu_B$ . The molecular orbital diagram for  $\text{Co}_2\text{YZ}$  Heusler compounds is presented in Figure 1 b by taking  $\text{Co}_2\text{MnAl}$  ( $N_v = 28$ ) as an example. The atomic  $d$  orbitals of  $[\text{CoZ}]$  ( $[\text{CoAl}]$ ) substructure and the second Co atom built two sets of  $t_{2g}$  and  $e_g$  hybrid orbitals. Y (Mn), which occupies the octahedral lattice site, adds its  $d$  states between these hybrid states. For  $\text{Co}_2\text{MnAl}$ , 24 valence electrons doubly occupy the orbitals, resembling the configuration of semiconducting  $\text{Fe}_2\text{VAl}$  ( $N_v = 24$ ), the additional 4 valence electrons singly occupy the  $e_g$  orbitals with parallel spin orientation owing to the small energy difference between the orbitals. This results in a half-metallic state and a  $M$  of  $4 \mu_B$  per formula unit. Similarly,  $\text{Co}_2\text{VGa}$ ,  $\text{Co}_2\text{VSn}$ ,  $\text{Co}_2\text{MnGa}$ ,  $\text{Co}_2\text{MnTi}$ , and  $\text{Co}_2\text{MnV}$ , which have  $N_v$  of 26, 27, 28, 29, and 30, also show half-metallic states with  $M$  of 2, 3, 4, 5, and  $6 \mu_B$  per formula unit, respectively (Figure 1 c). As the Co sites are in high spin states for all the investigated Heusler compounds, we are able to obtain the values of the local moment and  $e_g$  filling correspondingly (see Table S1 in the Supporting Information). More importantly, both the local magnetic

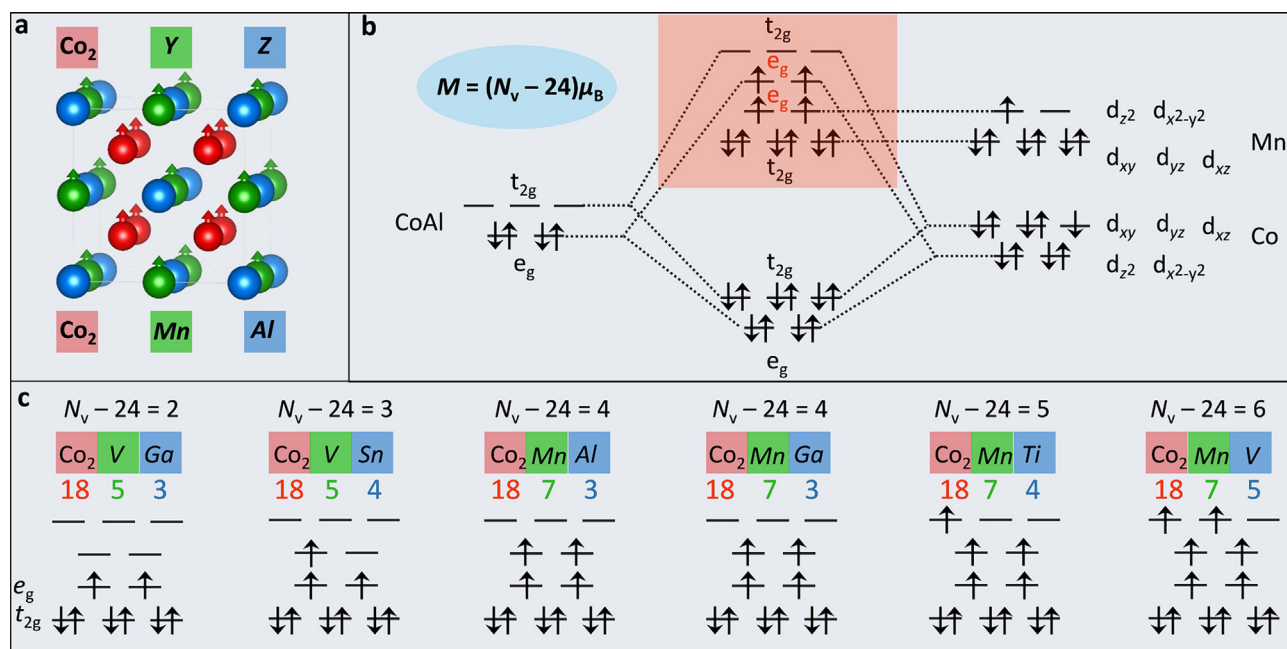


**Figure 1.** a) Crystal structure of  $\text{Co}_2\text{YZ}$  Heusler compounds. The magnetic moment  $M$  of  $\text{Co}_2\text{YZ}$  can be calculated according to the Slater-Pauling rule:  $M = (N_v - 24) \mu_B$ . b) Illustration of molecular orbital diagram of  $\text{Co}_2\text{MnAl}$ . c) The magnetic moment and electron occupation of the six selected  $\text{Co}_2\text{YZ}$  compounds. For simplicity, only the part (light red region) which presents different electron occupation is shown. The counting of valence electron number  $N_v$  is shown at the top.

moment and  $e_g$  filling of Co sites are not crystal surface-dependent (except the very first layer). This suggests a well-defined  $e_g$  orbital structure of Heusler compounds, making them a good platform for investigating the effect of electronic occupation in  $e_g$  orbitals on their catalytic performances.

Here, we selected  $\text{Co}_2$ -based Heusler compounds ( $\text{Co}_2\text{MnZ}$ ), i.e.,  $\text{Co}_2\text{MnAl}$ ,  $\text{Co}_2\text{MnTi}$ ,  $\text{Co}_2\text{MnGa}$ , and  $\text{Co}_2\text{MnV}$ , with different  $N_v$  and  $e_g$  filling, for OER study. It is not only due to the fact that Co as a 3d metal possesses varying  $e_g$  electron configuration with introducing different neighboring atoms, but also because of the high OER activity that Co-based catalysts have shown in the previous study.<sup>[15–18]</sup> All the compounds were first synthesized by arc-melting method into bulk crystals (Figure S1), which can be later cut into desired shapes.<sup>[2]</sup> As seen in Figure 2a–c,  $\text{Co}_2\text{MnGa}$  crystal was cut into a cuboid shape with the dimension of  $0.5 \times 0.5 \times 8 \text{ mm}^3$  that shows rough surfaces. Additionally, its mechanic robustness and metallic conductivity provide the great potential of such high-quality crystals in various applications including in electrocatalysis.

For detailed structural characterizations, the large crystals were treated with mechanical ball milling to form fine powders. X-ray diffraction (XRD) analysis was first employed to characterize the crystal structure of Heusler compounds. As shown in Figure 2d, powdered  $\text{Co}_2\text{MnGa}$  exhibits distinct reflections centered at  $20.0^\circ$ ,  $28.5^\circ$ ,  $35.0^\circ$ ,  $40.7^\circ$ , and  $45.8^\circ$  (2 theta value), corresponding to (220), (400), (422), (440), and (620) facets of  $\text{Co}_2\text{MnGa}$  cubic structure (PDF card: 27-1108).

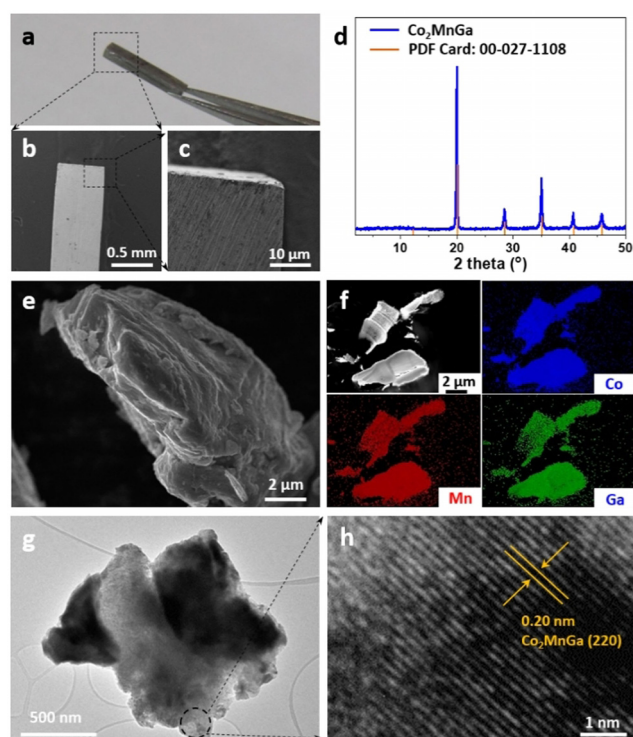


**Figure 2.** a) Digital image of  $\text{Co}_2\text{MnGa}$  crystal held by a tweezer. b,c) Low-resolution SEM images of  $\text{Co}_2\text{MnGa}$  single crystal. d) XRD pattern, e) SEM, f) elemental mapping, g) TEM, and h) HR-TEM images of powdered  $\text{Co}_2\text{MnGa}$  after ball-milling treatment.

The other compounds are also highly crystalline as demonstrated by the XRD patterns (Figure S2). It is worth mentioning that  $\text{Co}_2\text{VSn}$  and  $\text{Co}_2\text{MnTi}$  are not phase-pure, probably due to the impurities introduced by the processes of arc melting and ball-milling. This can be also seen from the elemental compositions of powdered Heusler compounds, as determined by energy-dispersive X-ray (EDX) spectroscopy. As shown in Figure S3, a small amount of impurity elements like Si, Fe, and Cr ( $\approx 2 \text{ at. \%}$ ) were found on each sample, as typically introduced by the synthesis procedures. Nevertheless, the major compositions are Co, Mn and Z (Ti, Al, V, Sn), and the atomic ratio of Co : Mn : Z is in good agreement with the stoichiometry in  $\text{Co}_2\text{MnZ}$  compounds, as seen in Table S2.

Electron microscopy was then conducted to visualize the surface morphology of powdered Heusler compounds. As shown in the scanning electron microscopy (SEM) images (Figure 2e and Figure S4), large crystals up to size of centimeters were milled into aggregates in the scale of micrometer. Elemental mapping images revealed the uniform distribution of Co, Mn, and Z (Ti, Al, V, and Ga), suggesting the high quality of Heusler crystals (Figure 2f and Figure S5–S7). A careful cutting on  $\text{Co}_2\text{MnGa}$  crystal allowed for direct imaging on the internal structure. As shown in Figure S8, single crystals were not grown into impermeable solid, instead, porosity was formed inside the crystals, in agreement with the observed rough surface in Figure 2c. Furthermore, transmission electron microscopy (TEM) images were taken for a closer observation of the crystal, as seen in Figure 2g and 2h. An overview TEM image shows that the average size of crystal domains is below  $2 \mu\text{m}$  (Figure S9). A representative crystal domain in Figure 2g is an aggregate of smaller crystalline particles. The observed lattice fringes in the high-resolution TEM image (Figure 2h) show a spacing of  $0.20 \text{ nm}$ , corresponding to the (220) planes of  $\text{Co}_2\text{MnGa}$  crystal. Moreover, spot EDX spectrum was collected to determine the local elemental ratio (Figure S10). The atomic ratio of Co : Mn : Ga is measured as  $2 : 1 : 1$ , perfectly matching with the stoichiometry in the  $\text{Co}_2\text{MnGa}$  compound.

To investigate the electrocatalytic activity of Heusler compounds,  $\text{Co}_2\text{MnZ}$  powder samples were deposited on glassy carbon (GC) electrode, and their OER activities were measured following the protocol proposed by the Jaramillo group.<sup>[6]</sup> Linear sweep voltammetry (LSV) was conducted to collect the polarization curves of  $\text{Co}_2\text{MnZ}$  compounds. As shown in Figure 3a, the catalytic activity of  $\text{Co}_2\text{MnZ}$  compounds has an obvious dependence on the Z element. Among them,  $\text{Co}_2\text{MnTi}$  delivered the highest current density. Similar activity was obtained with  $\text{Co}_2\text{MnAl}$  and  $\text{Co}_2\text{MnGa}$ , while the lowest current was achieved on the compound when Z is vanadium. The same trend could be observed on the corresponding Tafel slopes. In Figure 3b,  $\text{Co}_2\text{MnTi}$  as the most active sample showed the lowest value of Tafel slope ( $63 \text{ mV dec}^{-1}$ ), suggesting a more favorable catalytic kinetics. Almost the same Tafel slopes were obtained on  $\text{Co}_2\text{MnAl}$  ( $68 \text{ mV dec}^{-1}$ ) and  $\text{Co}_2\text{MnGa}$  ( $67 \text{ mV dec}^{-1}$ ) compounds. A typical value of Tafel slope of  $\approx 60 \text{ mV dec}^{-1}$  is generally reported for Co based catalysts where oxidized Co species determine the OER kinetics.<sup>[19–21]</sup> Similar Tafel slopes are



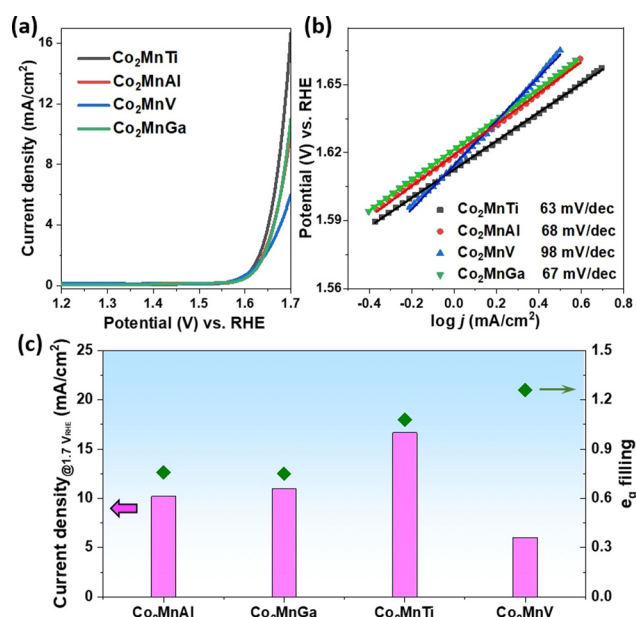


**Figure 3.** a) The LSV curves of Heusler compounds (Co<sub>2</sub>MnZ, Z = Ti, Al, V, and Ga). The current density was determined by the geometry surface area of the GC electrode (0.196 cm<sup>2</sup>). b) Tafel slopes derived from the LSV curves in (a) correspondingly. c) Comparison of current density at 1.7 V vs. RHE and  $e_g$  electron filling for Co<sub>2</sub>MnZ compounds. The current density was determined by the geometric surface area of the GC electrode (0.196 cm<sup>2</sup>).

observed on these Heusler compounds (63–68 mV dec<sup>-1</sup>) indicates that Co sites catalyze the OER process.

In addition, long-term stability of the Heusler compound was evaluated by applying a voltage of 1.63 V vs. RHE continuously for 12 h. As shown in Figure S11, Co<sub>2</sub>MnGa immobilized on carbon fiber paper as anode delivered a current density at around 2.5 mA cm<sup>-2</sup> with a continuous increase over 12 h. The electrode was further checked by SEM before and after stability test. As shown in Figure S12 and S13, Co<sub>2</sub>MnGa aggregates were robustly immobilized on electrode with the use of Nafion as a binder. A significant amount of Ga was leached out during measurement while Co and Mn were more resistant to the KOH electrolyte solution. In order to study alteration of the surface structure, we conducted a X-ray photoelectron spectroscopy (XPS) study on Co<sub>2</sub>MnGa before and after electrochemical test. In Figure S14, the survey of the XPS spectra indicated a similar chemical composition except that Ga was not detected on the surface after the electrochemical test. This is further supported by the disappeared peak in Ga 2p region (Figure S15c), which demonstrated surface leaching of Ga under applied voltage in alkaline electrolyte. On the other hand, Co and Mn were more resistant to electrolysis conditions. Nevertheless, significant oxidation was observed along with the formation of oxyhydroxide species on the surface during OER (Figure S15, a more detailed discussion is provided in supporting information). Therefore, the increase of current density could be attributed to surface oxidation/amorphization in alkaline electrolyte.<sup>[13,14]</sup> Furthermore, we are able to fabricate an electrode using a cuboid Co<sub>2</sub>MnGa

crystal directly. As seen in Figure S16, a single crystal of Co<sub>2</sub>MnGa is connected with inactive Ti wire by silver paste. For a small electrode (0.5 × 0.5 × 8 mm<sup>3</sup>), a substantial current (> 15 mA) was achieved at 1.7 V vs. RHE, demonstrating its potential as a practical electrode for efficient water electrolysis.

As mentioned, Z element influences the  $e_g$  electron configuration of Co through the covalent bonding, leading to precise regulation of  $e_g$  orbital filling. Considering the fact that both Mn and Z elements are not preferred active sites, Co sites are more efficient OER catalyst and in this work are key contributors to OER activity. Thus, we could correlate the OER activity of Co<sub>2</sub>MnZ compounds with the  $e_g$  orbital filling of reactive Co. As shown in Figure 3c, the catalytic performance of Co<sub>2</sub>MnAl and Co<sub>2</sub>MnGa can be associated with the values of the  $e_g$  filling, which are 0.76 and 0.75, respectively. When the  $e_g$  filling approached to unity (1.08), superior OER activity is achieved with Co<sub>2</sub>MnTi. Further increase of the  $e_g$  filling is not beneficial for OER catalysis, as illustrated by the lowest catalytic current delivered by Co<sub>2</sub>MnV catalyst ( $e_g$  filling: 1.26). Obviously, the OER activity of Heusler compounds shows a strong dependence on the  $e_g$  filling of reactive metal species.

To verify this dependence, another set of Heusler compounds (Co<sub>2</sub>VZ, Z = Sn and Ga) were synthesized following the same method. Detailed characterization confirms the good quality of Co<sub>2</sub>VZ crystals and their similar physical properties including surface morphology and domain size, as shown in Figure S17–S20. Employed as OER catalysts, Co<sub>2</sub>VSn is slightly more active with reaching a current density of 16.6 mA cm<sup>-2</sup> at 1.7 V vs. RHE, in comparison to Co<sub>2</sub>VGa (15 mA cm<sup>-2</sup>, Figure S21a). A reasonable Tafel slope (65 mV dec<sup>-1</sup>) is shown on both Co<sub>2</sub>VGa and Co<sub>2</sub>VSn compounds (Figure S21b). Figure 4 summarizes the OER activity of Co<sub>2</sub>MnZ and Co<sub>2</sub>VZ compounds, with plotting current density against the  $e_g$  orbital filling of reactive Co. A volcano-shaped curve was obtained, further supporting the dependence of OER activity on the  $e_g$  filling of reactive metal species in Heusler compounds. Moreover, we normalized the

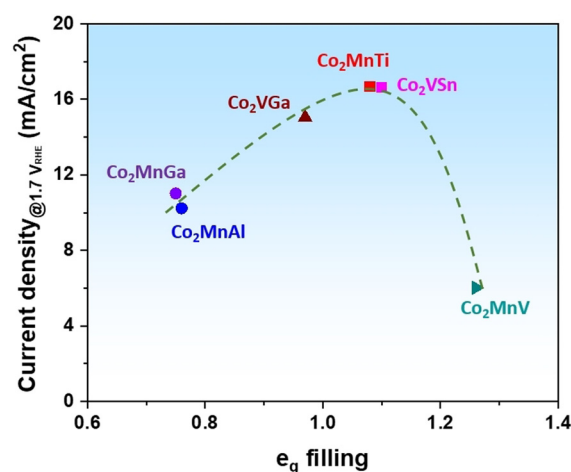


**Figure 4.** The volcano-shaped plot of the OER catalytic activity, defined by the current density at 1.7 V vs. RHE, against the occupancy of the  $e_g$  electron of Co in Heusler compounds (Co<sub>2</sub>MnZ and Co<sub>2</sub>VZ).

catalytic activity by the electrochemical surface area (ECSA) to compare the intrinsic activity of these Heusler compounds. As shown in Figure S22–23, a small value of double-layer capacitance ( $C_{dl}$ ; 2.4–3.2  $\mu\text{F}$ ) was obtained on all the Heusler compounds. Correspondingly, all the electrodes have a small ECSA (0.06–0.08  $\text{cm}^2$ ) due to the large particle size of crystals, in good agreement with the observation from electron microscopy. Upon normalization to ECSA, a volcano-shaped relation was also obtained between intrinsic OER activity and the  $e_g$  orbital filling of reactive Co (Figure S24), which reveals the regulation role of  $e_g$  orbital filling on Heusler catalysts.

It is widely accepted that the intrinsic activity of an OER catalyst is determined by the binding energy between surface metal sites and oxygen intermediates (e.g.  $^*\text{OH}$ ,  $^*\text{O}$ ,  $^*\text{OOH}$ , and  $^*\text{O}_2$ ).<sup>[22–24]</sup> Regulation on the  $e_g$  filling of surface metal ions could contribute to a more balanced binding energy and thus enhance OER activity, as proposed in SH principle and demonstrated by both experimental results and theoretical calculation in recent studies.<sup>[9,11,25,26]</sup> As demonstrated in this study, precise regulation of the  $e_g$  filling of Co sites can be achieved through tuning the elemental compositions of  $\text{Co}_2\text{YZ}$  Heusler compounds. A balanced adsorption/desorption bonding of oxygen intermediates is expected on optimized Heusler compounds with the  $e_g$  filling of Co sites approaching to unity. Resultantly,  $\text{Co}_2\text{MnTi}$ ,  $\text{Co}_2\text{VSn}$ , and  $\text{Co}_2\text{VGa}$  with  $e_g$  filling close to 1 are more efficient OER catalysts.

Furthermore, we studied the adsorption behavior of oxygen intermediates at the surface of  $\text{Co}_2\text{VSn}$  that exhibited the best OER activity among all the investigated Heusler compounds. Figure S25a depicts a general mechanism of OER on transition metal-based catalysts, in which the formation of  $^*\text{OOH}$  on metal sites is a crucial step.<sup>[24]</sup> Our theoretical calculation result suggests an unstable  $^*\text{OOH}$  intermediate on the surface Co sites (Figure S25b). Instead of coupling with hydroxyl anion to generate oxygen,  $^*\text{OOH}$  intermediate is immediately decomposed into  $^*\text{OH}$  and  $^*\text{O}$ . This indicates that a preferable OER pathway on Heusler compounds is via a direct combination of two M–O species with forming oxygen product and meanwhile releasing active sites. Thus, M–O bonding strength plays an important role on governing the overall OER kinetics on Heusler catalysts. For transition metals in the octahedral crystal field, the splitting of  $d$ -orbitals results in the formation of three  $t_{2g}$  and two  $e_g$  orbitals. Among which, only the  $e_g$  orbitals have a density of states that is out of the plane (Figure S25c), which enables an overlap with the O  $2p$  orbitals of oxygen intermediates (Figure S25d). As a result, tuning the  $e_g$  orbitals of Co sites could effectively modulate adsorption energy as well as electron transfer between surface cations and adsorbates towards a more efficient OER catalyst.<sup>[9,27,28]</sup>

In conclusion, high-quality crystals of Heusler compounds ( $\text{Co}_2\text{MnZ}$ ,  $Z = \text{Ti}$ ,  $\text{Al}$ ,  $\text{V}$ , and  $\text{Ga}$ ) were prepared by arc-melting method and were used as a new platform for electrochemical oxygen evolution reaction. The comparison on the OER activity illustrates a strong correlation with the  $e_g$  orbital filling of reactive Co sites and the optimal catalytic current was achieved when  $e_g$  orbital filling approached to

unity. This was further supported by another set of Heusler compounds ( $\text{Co}_2\text{VZ}$ ,  $Z = \text{Sn}$  and  $\text{Ga}$ ). Overall, the OER activity of Heusler compounds demonstrates a volcano-shaped dependence on  $e_g$  orbital filling of reactive transition metal cations. The theoretical calculation suggested a preferable OER pathway on Heusler compounds via a direct combination of two M–O species. Thus, tuning  $e_g$  orbital filling is an effective strategy to modulate the M–O bonding strength towards more active OER catalysts. This study not only explores the potential of Heusler compounds as novel OER electrocatalysts but also illustrates the optimization of catalysts based on precise regulation of electron configuration.

## Acknowledgements

We thank the Max Planck Society for basic funding. This work was financially supported by the IMPRS-RECHARGE of Max Planck Society and the Deutsche Forschungsgemeinschaft (DFG, German Research Foundation) Projektnummer 388390466-TRR 247 within the Collaborative Research Centre/Transregio 247 “Heterogeneous Oxidation Catalysis in the Liquid Phase”. This work was financially supported by the ERC Advanced Grant No. 291472 “Idea Heusler”, ERC Advanced Grant No. 742068 “TOPMAT”. We thank S. Palm, A. Kostis and A. Schlüter for EDX analysis and microscopy images. J. Ternieden is greatly acknowledged for conducting XRD measurements. We also thank S. Leiting and Dr. C. Weidenthaler for conducting XPS measurement and fruitful discussion. Open access funding enabled and organized by Projekt DEAL.

## Conflict of interest

The authors declare no conflict of interest.

**Keywords:** cobalt · heterogeneous catalysis · Heusler compounds · oxygen evolution reaction · water electrolysis

- [1] T. Graf, C. Felser, S. S. P. Parkin, *Prog. Solid State Chem.* **2011**, 39, 1–50.
- [2] K. Manna, L. Muechler, T. H. Kao, R. Stinshoff, Y. Zhang, J. Gooth, N. Kumar, G. Kreiner, K. Koepfner, R. Car, J. Kubler, G. H. Fecher, C. Shekhar, Y. Sun, C. Felser, *Phys. Rev. X* **2018**, 8, 041045.
- [3] C. J. Palmström, *Prog. Cryst. Growth Charact. Mater.* **2016**, 62, 371–397.
- [4] L. Wollmann, A. K. Nayak, S. S. P. Parkin, C. Felser, *Annu. Rev. Mater. Res.* **2017**, 47, 247–270.
- [5] S. Anand, K. Xia, V. I. Hegde, U. Aydemir, V. Kocovski, T. Zhu, C. Wolverton, G. J. Snyder, *Energy Environ. Sci.* **2018**, 11, 1480–1488.
- [6] C. C. McCrory, S. Jung, I. M. Ferrer, S. M. Chatman, J. C. Peters, T. F. Jaramillo, *J. Am. Chem. Soc.* **2015**, 137, 4347–4357.
- [7] I. Roger, M. A. Shipman, M. D. Symes, *Nat. Rev. Chem.* **2017**, 1, 0003.

- [8] X. Du, J. Huang, J. Zhang, Y. Yan, C. Wu, Y. Hu, C. Yan, T. Lei, W. Chen, C. Fan, J. Xiong, *Angew. Chem. Int. Ed.* **2019**, *58*, 4484–4502; *Angew. Chem.* **2019**, *131*, 4532–4551.
- [9] J. Suntivich, K. J. May, H. A. Gasteiger, J. B. Goodenough, Y. Shao-Horn, *Science* **2011**, *334*, 1383–1385.
- [10] J. Suntivich, H. A. Gasteiger, N. Yabuuchi, H. Nakanishi, J. B. Goodenough, Y. Shao-Horn, *Nat. Chem.* **2011**, *3*, 546–550.
- [11] Y. Tong, Y. Guo, P. Chen, H. Liu, M. Zhang, L. Zhang, W. Yan, W. Chu, C. Wu, Y. Xie, *Chem* **2017**, *3*, 812–821.
- [12] T. Kojima, S. Kameoka, S. Fujii, S. Ueda, A. P. Tsai, *Sci. Adv.* **2018**, *4*, eaat6063.
- [13] H.-J. Qiu, G. Fang, J. Gao, Y. Wen, J. Lv, H. Li, G. Xie, X. Liu, S. Sun, *ACS Mater. Lett.* **2019**, *1*, 526–533.
- [14] T. Löffler, A. Savan, A. Garzón-Manjón, M. Meischein, C. Scheu, A. Ludwig, W. Schuhmann, *ACS Energy Lett.* **2019**, *4*, 1206–1214.
- [15] A. Bergmann, T. E. Jones, E. M. Moreno, D. Teschner, P. Chernev, M. Glieth, T. Reier, H. Dau, P. Strasser, *Nat. Catal.* **2018**, *1*, 711–719.
- [16] M. W. Kanan, D. G. Nocera, *Science* **2008**, *321*, 1072–1075.
- [17] G. H. Moon, M. Yu, C. K. Chan, H. Tüysüz, *Angew. Chem. Int. Ed.* **2019**, *58*, 3491–3495; *Angew. Chem.* **2019**, *131*, 3529–3533.
- [18] M. Yu, G. H. Moon, R. G. Castillo, S. DeBeer, C. Weidenthaler, H. Tüysüz, *Angew. Chem. Int. Ed.* **2020**, *59*, 16544–16552; *Angew. Chem.* **2020**, *132*, 16687–16695.
- [19] M. Yu, C. K. Chan, H. Tüysüz, *ChemSusChem* **2018**, *11*, 605–611.
- [20] M. Yu, K. S. Belthle, C. Tüysüz, H. Tüysüz, *J. Mater. Chem. A* **2019**, *7*, 23130–23139.
- [21] Y. Surendranath, M. W. Kanan, D. G. Nocera, *J. Am. Chem. Soc.* **2010**, *132*, 16501–16509.
- [22] I. Katsounaros, S. Cherevko, A. R. Zeradjanin, K. J. Mayrhofer, *Angew. Chem. Int. Ed.* **2014**, *53*, 102–121; *Angew. Chem.* **2014**, *126*, 104–124.
- [23] N. T. Suen, S. F. Hung, Q. Quan, N. Zhang, Y. J. Xu, H. M. Chen, *Chem. Soc. Rev.* **2017**, *46*, 337–365.
- [24] F. Song, L. Bai, A. Moysiadou, S. Lee, C. Hu, L. Liardet, X. Hu, *J. Am. Chem. Soc.* **2018**, *140*, 7748–7759.
- [25] Y. Guo, Y. Tong, P. Chen, K. Xu, J. Zhao, Y. Lin, W. Chu, Z. Peng, C. Wu, Y. Xie, *Adv. Mater.* **2015**, *27*, 5989–5994.
- [26] X. Li, Y. Sun, Q. Wu, H. Liu, W. Gu, X. Wang, Z. Cheng, Z. Fu, Y. Lu, *J. Am. Chem. Soc.* **2019**, *141*, 3121–3128.
- [27] R. P. Forslund, W. G. Hardin, X. Rong, A. M. Abakumov, D. Filimonov, C. T. Alexander, J. T. Mefford, H. Iyer, A. M. Kolpak, K. P. Johnston, K. J. Stevenson, *Nat. Commun.* **2018**, *9*, 3150.
- [28] G. Li, Q. Xu, W. Shi, C. Fu, L. Jiao, M. E. Kamminga, M. Yu, H. Tüysüz, N. Kumar, V. Süß, R. Saha, A. K. Srivastava, S. Wirth, G. Auffermann, J. Gooth, S. Parkin, Y. Sun, E. Liu, C. Felser, *Sci. Adv.* **2019**, *5*, eaaw9867.

Manuscript received: October 9, 2020

Revised manuscript received: November 23, 2020

Accepted manuscript online: December 10, 2020

Version of record online: February 3, 2021